Relating Phenomenology to Measurement Matrix for Dropped Channel Polarimetric SAR

Julie Ann Jackson
Air Force Institute of Technology
Dayton, Ohio
UNITED STATES

Forest Lee-Elkin
Felkintech, LLC
Dayton, Ohio
UNITED STATES

julie.jackson@afit.edu

felkintech@gmail.com

ABSTRACT

Previously, we have introduced dropped channel polarimetric synthetic aperture radar, which uses compressive sensing (CS) to reconstruct full-pol imagery from a sub-set of measured channels. A key feature of the method is the channel mixing that occurs via channel coupling, either naturally via antenna and feedline crosstalk or via active components. This paper considers elements of the sparse recovery problem in relation to physical phenomenology. Specifically, this paper discusses the channel coupling matrix, the channel selection matrix, and the target reflectivity coefficients to be estimated. Coupling matrix elements depend on coupling at both the transmitter and receiver. Previous work randomly selected coupling coefficients to minimize mutual coherence of the measurement matrix. Here, we examine structure imposed by radar system properties and demonstrate dropped channel polarimetric SAR through a series of examples.

1.0 INTRODUCTION

Typically polarization channel and antenna crosstalk is minimized during radar design, and residual crosstalk correction is achieved by applying the inverse of the crosstalk matrix to the full channel data. However, antenna crosstalk provides channel mixing that enables compressive sensing (CS) across polarization channels.

CS for radar has generally focused on slow-time and/or fast-time under-sampling and randomization [1-7]. Polarimetric CS [4, 8 Ch. 7] has not accounted for different sparsity support on each channel and has not reduced the number of channel measurements. Our model [9-11] recognizes the unavoidable existence of antenna crosstalk and uses it to reduce the number of channel measurements required for polarimetric synthetic aperture radar (PolSAR).

This paper summarizes the theoretical development of the dropped-channel PolSAR CS model from [9-13] and discusses factors regarding channel coupling and channel selection. Example results using the AFRL GOTCHA data set [14] are shown as proof of concept for a variety of relevant radar configurations. Additional analysis and references may be found in [9-11].

2.0 DROPPED-CHANNEL POLSAR CS

Dropped-channel PolSAR measures only M of M' available polarization channels and uses antenna coupling and basis pursuit denoising (BPDN) to recover the unmeasured channel, remove point spread effects, and obtain polarimetric scattering information [9-13]. An example radar system configuration is shown in Figure 1. The measured images, scene reflectivity to be estimated, and BPDN recovery are defined as follows.
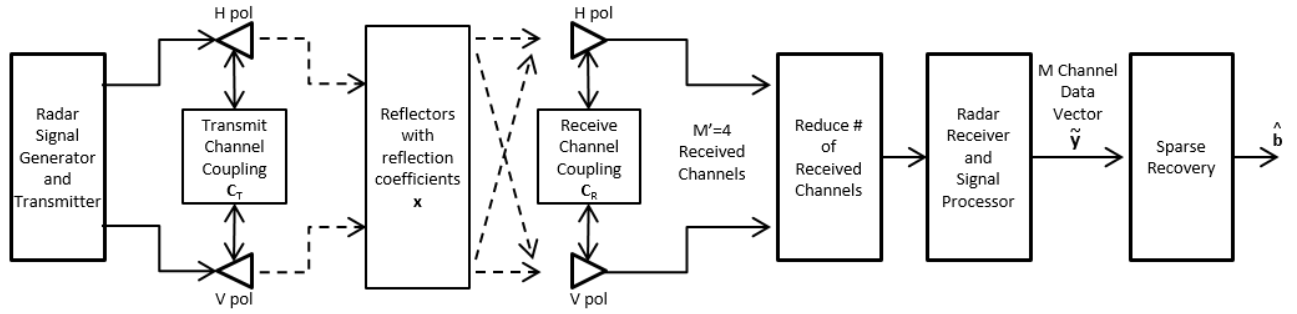
Figure 1: POLSAR CS system overview

In (1) below, we follow [9] and update the model from [10-12] to omit additive noise and instead include scene clutter since we expect SAR images to be clutter-limited, that is, to have clutter power much larger than thermal noise. Working in the spatial domain, vectorized scene reflectivity $\mathbf{x}_m \in \square^{N'\times 1}$ with N' unknown reflectivity values for the mth measured channel is mapped to a vectorized image $\mathbf{y}_m \in \square^{N\times 1}$ with N pixels via convolution with the point spread function, represented by $\mathbf{y}_m = \mathbf{A}_m \mathbf{x}_m$. Stacking the M' reflectivity channels such that $\mathbf{x} = [\mathbf{x}_1,\ldots,\mathbf{x}_{M'}]^T$ and the $M \le M'$ measured channels such that $\tilde{\mathbf{y}} = [\mathbf{y}_1,\ldots,\mathbf{y}_M]^T \in \square^{MN\times 1}$ and including clutter $\mathbf{w} \in \square^{M'N'\times 1}$, the multi-channel measured signal model can be written as [9]

$$\tilde{\mathbf{y}} = \tilde{\mathbf{A}}_M (\mathbf{JC} \otimes \mathbf{I}_{N'})(\mathbf{x} + \mathbf{w})$$

(1)

where $\otimes$ denotes the Kronecker product, $\mathbf{C} \in \square^{M'\times M'}$ is the complex channel coupling matrix, matrix $\mathbf{J} \in \square^{M\times M'}$ is a channel selection matrix, and $\mathbf{I}_{N'}$ is the $N'\times N'$ identity matrix. Furthermore, $\tilde{\mathbf{A}}_M$ is a block diagonal matrix of point spread convolution operators $\mathbf{A}_m$ for the M measured channels.

The $M'\times M'$ channel coupling matrix $\mathbf{C}$ captures crosstalk that occurs at both the transmit and receive antennas. In general $\mathbf{C}$ is complex-valued to account for both magnitude and phase interactions. Physical structure of $\mathbf{C}$ is discussed further in Section 3.1.2 below. Typically, crosstalk is considered an undesirable degradation of signals. However, we exploit the mixing of channels to reduce the number of channel measurement required. Channel selection matrix $\mathbf{J}$ drops or further mixes channels to reduce from M' reflectivity channels to $M<M'$ measured channels. Note, as shown in Figure 1, channel reduction comes between the receive antenna and receive signal processing steps. Channel selection is further discussed in Section 3.1.3.

If prior knowledge of the scene, or some intelligence as to what types of targets are expected is available, it can be beneficial to decompose reflectivity $\mathbf{x}$ into a dictionary times a coefficient vector as

$$\mathbf{x} = (\mathbf{P} \otimes \mathbf{S})\mathbf{b}$$

(2)

where $\mathbf{P} \in \square^{M'\times Q}$ is a dictionary containing Q polarization responses, $\mathbf{S} \in \square^{N'\times S'}$ is a dictionary matched to scatterer spatial responses of interest and $\mathbf{b} \in \square^{QS'\times 1}$ is a coefficients vector. If $\mathbf{P}$ and $\mathbf{S}$ are selected

appropriately, the scene can be reconstructed from a sparse set of coefficients in **b**.

To recover the sparse coefficients **b**, we solve the BPDN problem

$$\min_{\mathbf{b}} \|\mathbf{b}\|_1 \text{ s.t.} \left\| \tilde{\mathbf{y}} - \tilde{\mathbf{A}}_M (\mathbf{JC} \otimes \mathbf{I}_{N'})(\mathbf{P} \otimes \mathbf{S})\mathbf{b} \right\|_2 \leq \epsilon$$

(3)

using the *spgl1* algorithm [15, 16]. When **b** is recovered perfectly, the ℓ_2-norm fit constraint reduces to the norm of the imaged clutter: $\left\| \tilde{\mathbf{A}}_M (\mathbf{JC} \otimes \mathbf{I}_{N'})\mathbf{w} \right\|_2 \leq \epsilon$. That is, recovery is limited by the power of the clutter in the image domain. As such, we set the BPDN error radius ϵ such that the ℓ_2 norm of the imaged clutter lies within the epsilon ball with 95% probability.

Figures 2 and 3 show examples from [9] on the AFRL GOTCHA data set [14] to illustrate simultaneous channel (and thus polarimetric information) recovery and point spread removal is possible in the proposed framework. The polarimetric responses are presented in Cyan-Magenta-Yellow (CMY) pseudo-colors that map to polarimetric response types in dictionary **P**, as noted in the colormap legends. Additional examples will be presented in Section 4.

3.0 POLSAR CS DESIGN CONSIDERATIONS

For any CS problem, recovery performance depends on the design of the measurement matrix and signal dictionary. In this section, we discuss how the measurement matrix and signal dictionary relate to the elements of the PolSAR system in Figure 1.

3.1 Measurement Matrix

For the PolSAR system in Figure 1, the measurement matrix models the mapping from reflectivity **x** to measurements **y**. For SAR imaging, the mapping includes convolution with the point spread function, transmit and receive antenna coupling, and channel selection for data compression.

3.1.1 Point Spread Function

A linear time invariant system model for SAR imaging describes the image domain response as the convolution of a point spread function (psf) with the scene reflectivity function, which characterizes the electromagnetic scattering coefficients of objects in the scene. The psf is determined by the spatial frequency (phase history) domain support of the radar data collection, including radar operating frequency, bandwidth, look angle, and aperture extent. The psf can be modelled as the inverse Fourier transform of the spatial frequency support: $\mathbf{h} = F^{-1}\{\mathbf{H}\}$. For multiple polarization channels, the support may vary, resulting in multiple psfs $\mathbf{h}_m$. The operator $\mathbf{A}_m$ to convolve psf with reflectivity may be written in matrix form using samples of the psf for each channel. Then, $\tilde{\mathbf{A}}_M$ is a block diagonal matrix of the $\mathbf{A}_m$ operators:

$$\tilde{\mathbf{A}}_M = \begin{bmatrix} \mathbf{A}_1 & 0 & 0 \\ 0 & \ddots & 0 \\ 0 & 0 & \mathbf{A}_M \end{bmatrix},$$

(4)

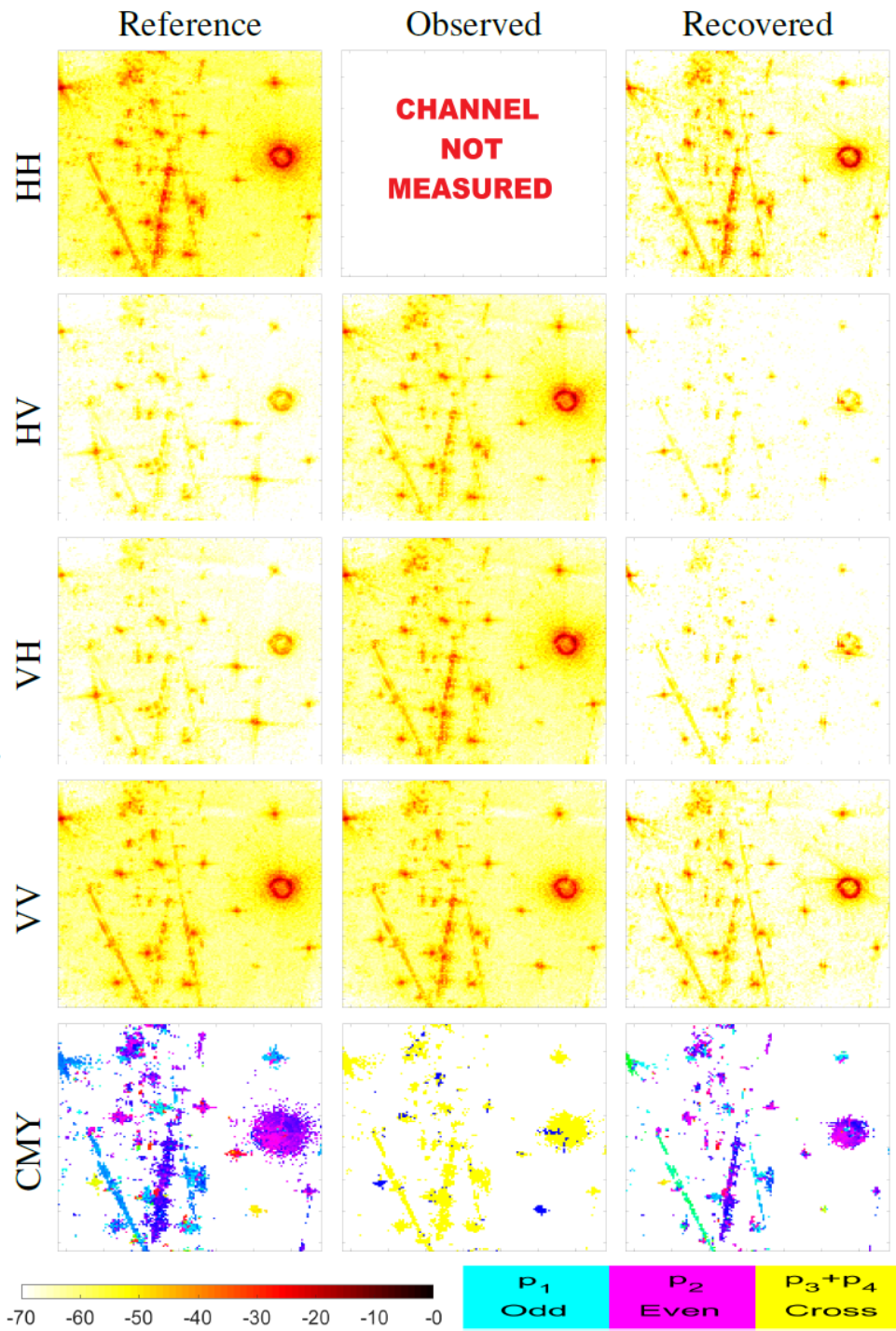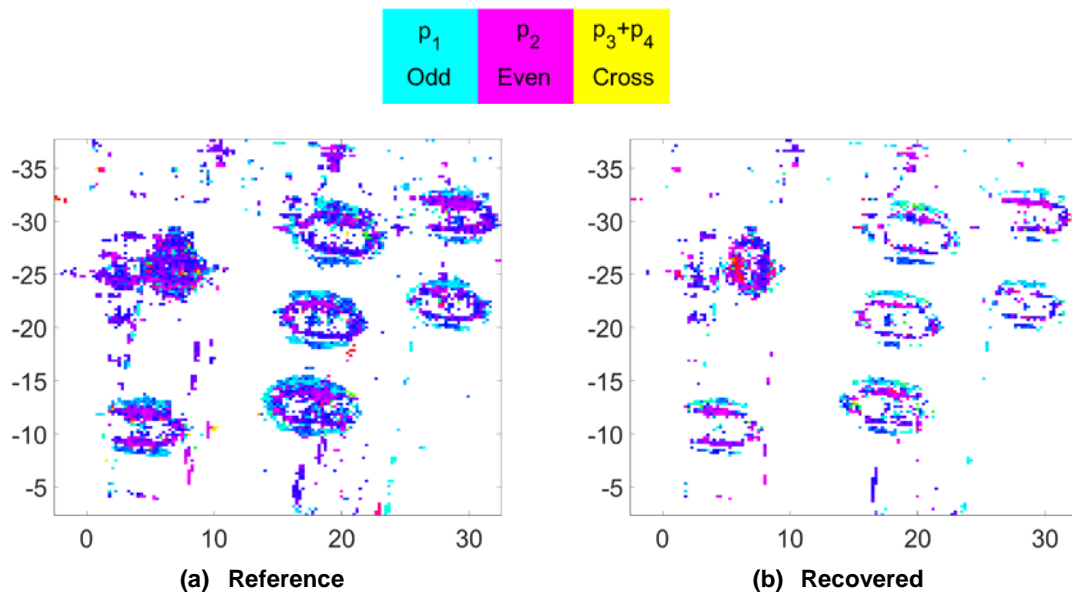where in (1), only the *M* measured channel psfs are included in $\tilde{\mathbf{A}}_M$

Figure 2: Reference, Observed, and Recovered images of calibration targets for 360° aperture reconstructed from combined 5° subapertures with P=P$_{Pauli}$ and HH channel not observed.

**Figure 3: Comparison of CMY polarimetric pseudo-color images of GOTCHA vehicles for 360°
aperture reconstructed from combined 5° subapertures with P=P$_{Pauli}$ and HH channel not
observed.**

.3.1.2   Antenna Coupling

The key to successful CS is a linear mixing of information to be recovered in the measurement set. In our application, the antenna or channel coupling matrix provides the requisite mixing. As shown in Figure 1, channel coupling occurs on both transmit and receive. The figures illustrates a two channel polarimetric system with horizontal (H) and vertical (V) polarized antennas, but other polarizations may be used, such as left and right circular. For ease of discussion, we refer to H and V polarization.

The system in Figure 1 transmits a signal $s_H(t)$ on the H channel and a signal $s_V(t)$ on the V channel. Inevitably, some fraction of $s_H(t)$ will couple into the V antenna, and some portion of $s_V(t)$ will couple into the H antenna. Interaction with a scatterer will induce on the transmitted field a reflection coefficient (γ) that includes both a scale factor and a rotation of the electric field. The amount of rotation will depend on the object's material, shape, and orientation relative to the radar [17]. Thus, the both radar receive antennas may collect scaled versions of either $s_V(t)$ or $s_H(t)$.

Let t_{HH} and t_{VV} denote the gains on the H and V transmit channels, respectively. Further, let t_{HV} denote the coupling (amplitude and phase) of $s_H(t)$ onto the V transmit channel and t_{VH} denote the coupling of $s_V(t)$ onto the H transmit channel. Similarly, define gains and coupling coefficients for the receiver. Then, the overall coupling matrix for the system may be written as

$$\mathbf{C} = \mathbf{C}_{\mathrm{T}} \otimes \mathbf{C}_{\mathrm{R}}^{T}$$

$$= \begin{bmatrix} t_{\mathrm{HH}} & t_{\mathrm{HV}} \\ t_{\mathrm{VH}} & t_{\mathrm{VV}} \end{bmatrix} \otimes \begin{bmatrix} r_{\mathrm{HH}} & r_{\mathrm{VH}} \\ r_{\mathrm{HV}} & r_{\mathrm{VV}} \end{bmatrix} \tag{5}$$

$$= \begin{bmatrix} t_{\mathrm{HH}}r_{\mathrm{HH}} & t_{\mathrm{HH}}r_{\mathrm{VH}} & t_{\mathrm{HV}}r_{\mathrm{HH}} & t_{\mathrm{HV}}r_{\mathrm{VH}} \\ t_{\mathrm{HH}}r_{\mathrm{HV}} & t_{\mathrm{HH}}r_{\mathrm{VV}} & t_{\mathrm{HV}}r_{\mathrm{HV}} & t_{\mathrm{HV}}r_{\mathrm{VV}} \\ t_{\mathrm{VH}}r_{\mathrm{HH}} & t_{\mathrm{VH}}r_{\mathrm{VH}} & t_{\mathrm{VV}}r_{\mathrm{HH}} & t_{\mathrm{VV}}r_{\mathrm{VH}} \\ t_{\mathrm{VH}}r_{\mathrm{HV}} & t_{\mathrm{VH}}r_{\mathrm{VV}} & t_{\mathrm{VV}}r_{\mathrm{HV}} & t_{\mathrm{VV}}r_{\mathrm{VV}} \end{bmatrix}.$$

There are sixteen possible paths through the transmitter-target-receiver path, as summarized in Table 1. Thus, the received signals at the H and V channels may be written as

$$\begin{bmatrix} s_{HH}(t) \\ s_{HV}(t) \\ s_{VH}(t) \\ s_{VV}(t) \end{bmatrix} = \begin{bmatrix} t_{\mathrm{HH}}s_H(t)r_{\mathrm{HH}} & t_{\mathrm{HH}}s_H(t)r_{\mathrm{VH}} & t_{\mathrm{HV}}s_H(t)r_{\mathrm{HH}} & t_{\mathrm{HV}}s_H(t)r_{\mathrm{VH}} \\ t_{\mathrm{HH}}s_H(t)r_{\mathrm{HV}} & t_{\mathrm{HH}}s_H(t)r_{\mathrm{VV}} & t_{\mathrm{HV}}s_H(t)r_{\mathrm{HV}} & t_{\mathrm{HV}}s_H(t)r_{\mathrm{VV}} \\ t_{\mathrm{VH}}s_V(t)r_{\mathrm{HH}} & t_{\mathrm{VH}}s_V(t)r_{\mathrm{VH}} & t_{\mathrm{VV}}s_V(t)r_{\mathrm{HH}} & t_{\mathrm{VV}}s_V(t)r_{\mathrm{VH}} \\ t_{\mathrm{VH}}s_V(t)r_{\mathrm{HV}} & t_{\mathrm{VH}}s_V(t)r_{\mathrm{VV}} & t_{\mathrm{VV}}s_V(t)r_{\mathrm{HV}} & t_{\mathrm{VV}}s_V(t)r_{\mathrm{VV}} \end{bmatrix} \begin{bmatrix} \gamma_{HH} \\ \gamma_{HV} \\ \gamma_{VH} \\ \gamma_{VV} \end{bmatrix} \tag{6}$$

where the first subscript on $s(t)$ on the left-hand side of (6) denotes the transmitted field polarization and the second subscript denotes the receive antenna polarization.

Typically, all four received signals $s_{HH}(t)$, $s_{HV}(t)$, $s_{VH}(t)$, and $s_{VV}(t)$ get match filtered, sampled, etc. by the radar receiver and signal processor into phase history data and subsequent image stack $\mathbf{y}$. Under the isotropic point assumption inherent in SAR image theory, the reflection coefficients γ_{HH}, γ_{HV}, γ_{VH}, γ_{VV} map to the unknown reflectivity $\mathbf{x}$, which we estimate using BPDN.

The coupling matrix $\mathbf{C}$ in (5) captures the mixing of information to be recovered ($\mathbf{x}$) and enables a CS framework. Thus, our approach selects a subset of received signals to process into images. Optimal design of channel selection in conjunction with coupling matrix $\mathbf{C}$ will improve recovery performance. Design considerations include physical antenna properties, proximity of channel hardware, power limitations, and reciprocity. Reciprocity requires $\mathbf{C}_T$ and $\mathbf{C}_R$ to be symmetric. Symmetry can only be broken if an active coupling component is introduced. We show examples of channel recovery using both passive and active coupling in Section 4.

Table 1: Summary of the sixteen possible paths through the transmitter-target-receiver path.

Channels	Description	Coefficients
HH	Transmit $s_H(t)$, target maintains H, receiver gain on H	$t_{HH}s_H(t)\gamma_{HH}r_{HH}$
	Transmit $s_H(t)$, target flips to V, receiver receives fraction of V pol on H channel	$t_{HH}s_H(t)\gamma_{HV}r_{VH}$
	Fraction of transmitted $s_H(t)$ that emits on V channel, target flips to H, receiver gain on H	$t_{HV}s_H(t)\gamma_{VH}r_{HH}$
	Fraction of transmitted $s_H(t)$ that emits on V channel, target maintains V, receiver receives fraction of V pol on H channel	$t_{HV}s_H(t)\gamma_{VV}r_{VH}$
HV	Transmit H, target maintains H, receiver receives fraction of H pol on V channel	$t_{HH}s_H(t)\gamma_{HH}r_{HV}$
	Transmit H, target flips to V, receiver gain on V	$t_{HH}s_H(t)\gamma_{HV}r_{VV}$
	Fraction of transmitted H that emits on V channel, target flips to H, receiver receives fraction of H pol on V channel	$t_{HV}s_H(t)\gamma_{VH}r_{HV}$
	Fraction of transmitted H that emits on V channel, target maintains V, receiver gain on V	$t_{HV}s_H(t)\gamma_{VV}r_{VV}$
VH	Fraction of transmitted V that emits on H channel, target maintains H, receiver gain on H	$t_{VH}s_V(t)\gamma_{HH}r_{HH}$
	Fraction of transmitted V that emits on H channel, target flips to V, receiver receives fraction of V pol on H channel	$t_{VH}s_V(t)\gamma_{HV}r_{VH}$
	Transmit V, target flips to H, receiver gain on H	$t_{VV}s_V(t)\gamma_{VH}r_{HH}$
	Transmit V, target maintains V, receiver receives fraction of V pol on H channel	$t_{VV}s_V(t)\gamma_{VV}r_{VH}$
VV	Fraction of transmitted V that emits on H channel, target maintains H, receiver receives fraction of H pol on V channel	$t_{VH}s_V(t)\gamma_{HH}r_{HV}$
	Fraction of transmitted V that emits on H channel, target flips to V, receiver gain on V	$t_{VH}s_V(t)\gamma_{HV}r_{VV}$
	Transmit V, target flips to H, receiver receives fraction of H pol on V channel	$t_{VV}s_V(t)\gamma_{VH}r_{HV}$
	Transmit V, target maintains V, receiver gain on V	$t_{VV}s_V(t)\gamma_{VV}r_{VV}$

3.1.3   Channel Selection

Channel selection compresses the PolSAR data by dropping received signal channels. The proposed approach may be combined with slow-time and/or fast time CS sampling schemes, but here, we focus on reduction of polarization channels only. The channel selection operator **J** in (1) may be used to drop channels or further mix them. For dropping channels, J is formed by removing the dropped-channel rows from an identity matrix. For example, to drop the HH channel

$$\mathbf{J} = \begin{bmatrix} 0 & 1 & 0 & 0 \\ 0 & 0 & 1 & 0 \\ 0 & 0 & 0 & 1 \end{bmatrix}. \tag{7}$$

Often, monostatic radar is thought to have three polarizations because the HV and VH channels are considered equal due to reciprocity. However, in practice, the collected HV and VH channels may be averaged to reduce the data burden from four channels to three. In that case, the channel selection operator may be written as

$$\mathbf{J} = \begin{bmatrix} 1 & 0 & 0 & 0 \\ 0 & 0.5 & 0.5 & 0 \\ 0 & 0 & 0 & 1 \end{bmatrix} \tag{8}$$

Further reduction of channels for CS may be achieved by dropping a row from (8). Examples for a variety of channel selection cases are shown in Section 4.

3.2   Sparse Dictionary Representation

In addition to the measurement matrix, CS recovery depends on the signal **x** being sparse in some dictionary. Reflectivity **x** may be decomposed as in (2) into a polarization dictionary that encodes scatterer polarimetric

channel relations and a spatial dictionary that encodes scatterer spatial extent, location, and orientation.

3.2.1 Polarization Dictionary

The Pauli basis

$$\mathbf{P}_{\text{Pauli}} = \frac{1}{\sqrt{2}} \begin{bmatrix} 1 & 1 & 0 & 0 \\ 0 & 0 & 1 & -j \\ 0 & 0 & 1 & j \\ 1 & -1 & 0 & 0 \end{bmatrix} \tag{9}$$

is often used to describe the scattering response of canonical scatterers [17]. The first and fourth row correspond to the co-pol responses HH and VV. The second and third rows correspond to the cross-pol responses HV and VH. The first column corresponds to odd-bounce scatterers such as a plate or trihedral. The second column corresponds to even-bounce scatterers such as a dihedral or top-hat. A dihedral oriented with its seam rotated 45° about the radar line of sight will result in the cross-pol response in the third column, and the fourth column corresponds to a helical scatterer. Other dictionaries may be used but should be matched to objects expected in the scene to enable a sparse representation.

3.2.2 Spatial Dictionary

Point target or extended target dictionaries may be used to balance signal fit and sparsity in (3). In this paper, we assume an isotropic point model, so $\mathbf{S}=\mathbf{I}_{4x4}$. Examples of an extended target dictionary may be found in [12].

4.0 EXAMPLES

Optimal design of the measurement and dictionary matrices will improve sparse reconstruction. However, even sub-optimal designs can produce good results. In this section, we show polarimetric pseudo-color images recovered using BPDN on mixed channel data generated using the AFRL GOTCHA data set [14]. The Pauli polarization dictionary and isotropic point spatial dictionary are used in each case. Complex coupling coefficients are listed as amplitude and phase angle in radians. Results show reasonable sparse reconstruction for several key radar configurations, including active coupling, passive coupling, dropping one channel, and dropping two channels. These results should improve in the future commensurate with improvements in the design of the radar coupling matrix.

4.1 Antenna Coupling Matrix Structure

Figure 4 shows recovery of a top-hat and a vehicle target in the GOTCHA scene for different coupling matrices and measurements of the HV, VH, and VV channels only (HH dropped). The first column provides a reference image generated using the original (no crosstalk coupling) four-channel polarimetric data. The second column uses coupling matrix $\mathbf{C}$ with off-diagonal entries generated with uniform random amplitudes in [0,1] and uniform random phase in [0,2π]. Although the random $\mathbf{C}$ fits well with CS theory, physical structure dictated by antenna theory and the radar model in Figure 1 result in the Kronecker product structure of (5). The third column of Figure 4 demonstrates that recovery is possible even within the structure of (5). Finally, the fourth column of Figure 4 shows that removing active coupling components and further restricting transmit and receive components of $\mathbf{C}$ to be symmetric for reciprocity still allows for good recovery. Improved recovery will be possible upon optimization of $\mathbf{C}$.
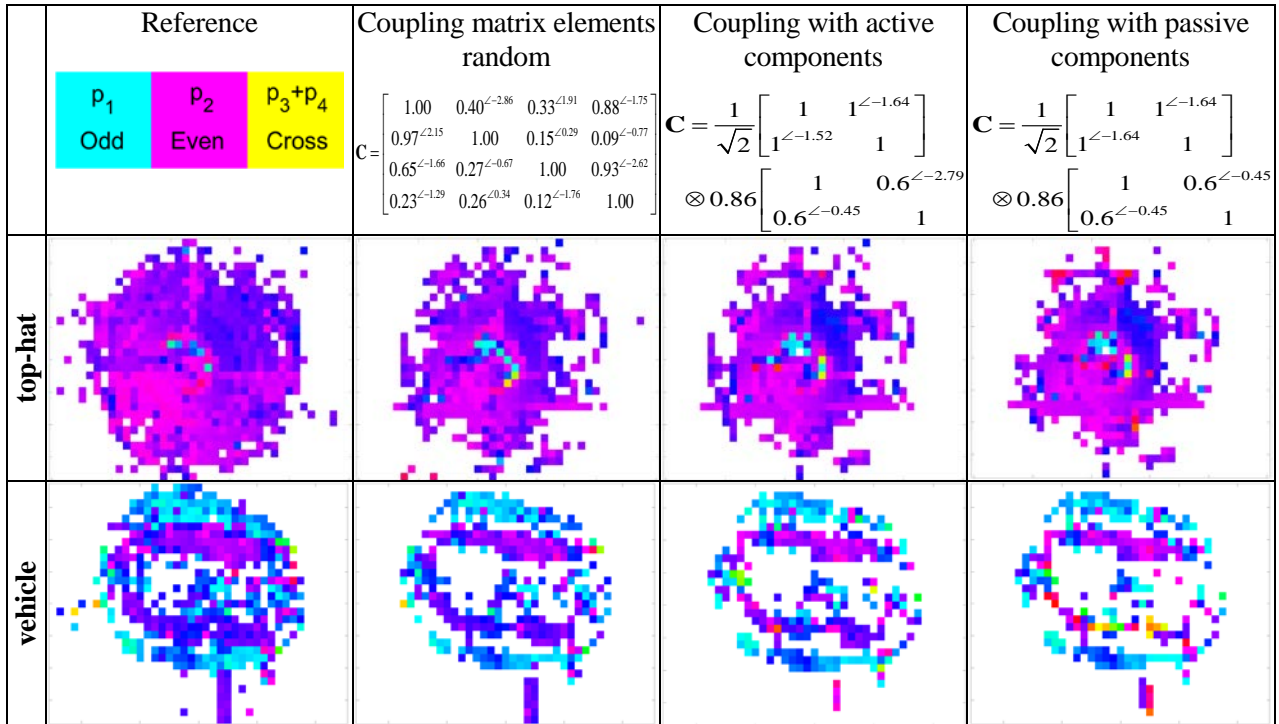
Figure 4: Top-hat and vehicle recovery using different coupling matrices (HH dropped).

4.2   Channel Selection

Figures 5 and 6 show recovery of the top-hat and vehicle for different channel selection matrices $\mathbf{J}$. In Figure 5, the $\mathbf{C}$ matrix is the same as for column 3 of Figure 4, the active coupling case. In Figure 5, the "Drop HH Channel" result is the same case as Figure 4 column 3. Variation in performance in Figure 5 is due to lack of optimization of $\mathbf{C}$ in conjunction with $\mathbf{J}$; however, most cases recover the polarimetric information fairly well. Figure 6 recoveries with two channels dropped are degraded but still reasonable, with the double-bounce and single bounce rings distinguishable and closer to the true polarimetric response than not. We have included the familiar monostatic case with averaged HV and VH channels in columns 4 and 5 of Figure 6, with column 5 also dropping the HH channel. Again, appropriate design of coupling matrix $\mathbf{C}$ will improve recovery of polarimetric information in addition to the sparse spatial reconstruction.
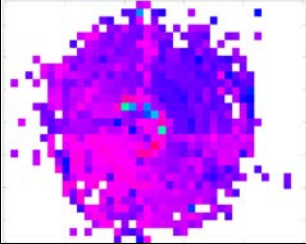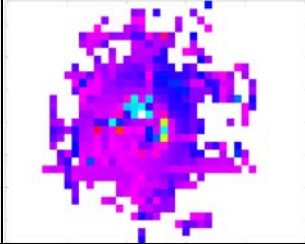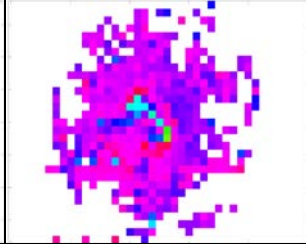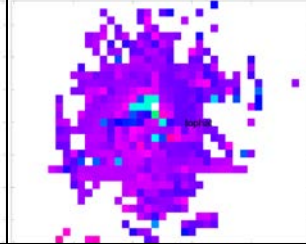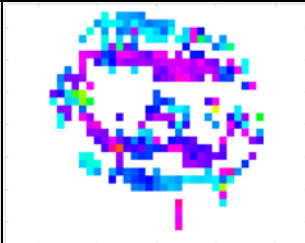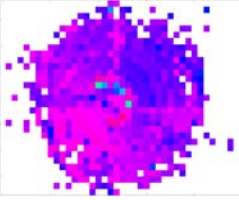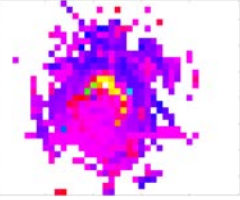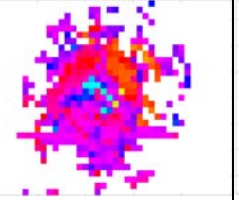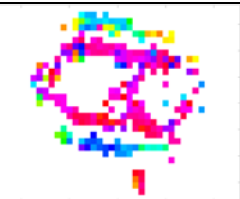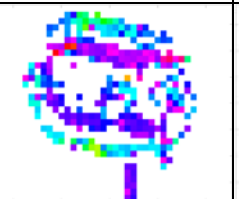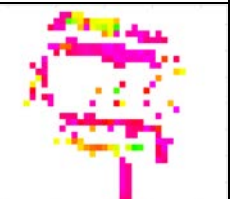
	Reference	Drop HH Channel	Drop HV Channel	Drop VV Channel
	p_1 Odd $\quad$ p_2 Even $\quad$ p_3+p_4 Cross	$\mathbf{J} = \begin{bmatrix} 0 & 1 & 0 & 0 \\ 0 & 0 & 1 & 0 \\ 0 & 0 & 0 & 1 \end{bmatrix}$	$\mathbf{J} = \begin{bmatrix} 1 & 0 & 0 & 0 \\ 0 & 0 & 1 & 0 \\ 0 & 0 & 0 & 1 \end{bmatrix}$	$\mathbf{J} = \begin{bmatrix} 1 & 0 & 0 & 0 \\ 0 & 1 & 0 & 0 \\ 0 & 0 & 1 & 0 \end{bmatrix}$
top-hat				
vehicle				

Figure 5: Top-hat and vehicle recovery using different channel selections with one channel dropped (active coupling case (col. 3, Fig. 4):

$$\mathbf{C} = \frac{1}{\sqrt{2}} \begin{bmatrix} 1 & 1^{\angle -1.64} \\ 1^{\angle -1.52} & 1 \end{bmatrix} \otimes 0.86 \begin{bmatrix} 1 & 0.6^{\angle -2.79} \\ 0.6^{\angle -0.45} & 1 \end{bmatrix}).$$

5.0 CONCLUSION

This paper presented examples of dropped-channel PolSAR CS for different channel coupling and channel selection cases whose structure results from radar physics and system factors. More detail on the model and additional examples may be found in [9-13]. Future work will consider optimization of the measurement matrix for improved reconstruction.

	Reference	Drop HH and VV Channels	Drop HH and VH Channels	Monostatic averaging of HV and VH Channels;	Monostatic averaging of HV and VH Channels; drop HH
	p_1 Odd, p_2 Even, p_3+p_4 Cross	$\mathbf{J} = \begin{bmatrix} 0 & 1 & 0 & 0 \\ 0 & 0 & 1 & 0 \end{bmatrix}$	$\mathbf{J} = \begin{bmatrix} 0 & 1 & 0 & 0 \\ 0 & 0 & 0 & 1 \end{bmatrix}$	$\mathbf{J} = \begin{bmatrix} 1 & 0 & 0 & 0 \\ 0 & 0.5 & 0.5 & 0 \\ 0 & 0 & 0 & 1 \end{bmatrix}$	$\mathbf{J} = \begin{bmatrix} 0 & 0.5 & 0.5 & 0 \\ 0 & 0 & 0 & 1 \end{bmatrix}$
top-hat					
vehicle					

Figure 6: Top-hat and vehicle recovery using different channel selections with two channels dropped or combined. Coupling matrix for all cases is

$$\mathbf{C} = 0.78 \begin{bmatrix} 1 & 0.8^{\angle 3.03} \\ 0.91^{\angle 0.29} & 0.91 \end{bmatrix} \otimes 0.93 \begin{bmatrix} 1 & 0.4^{\angle -1.63} \\ 0.4^{\angle -1.63} & 1 \end{bmatrix}.$$

6.0   REFERENCES

[1]   V. M. Patel, G. R. Easley, D. M. Healy Jr., and R. Chellappa, "Compressed synthetic aperture radar," IEEE Journal of Selected Topics in Signal Processing, vol. 4, no. 2, pp. 244–254, April 2010.

[2]   J. Xu, Y. Pi, and Z. Cao, "Bayesian compressive sensing in synthetic aperture radar imaging," IET Radar Sonar and Navigation, vol. 6, no. 1, pp. 2–8, 2012.

[3]   R. Baraniuk and P. Steeghs, "Compressive radar imaging," in IEEE Radar Conf., 2007, pp. 128–133.

[4]   W. Qiu, H. Zhao, J. Zhou, and Q. Fu, "High-resolution fully polarimetric ISAR imaging based on compressive sensing," IEEE Trans. on Geoscience and Remote Sensing, vol. 52, no. 10, pp. 6119–6131, Oct. 2014.

[5]   K. Aberman and Y. C. Eldar, "Sub-nyquist SAR via Fourier domain range-doppler processing," IEEE Trans. on Geoscience and Remote Sensing, vol. 55, no. 11, pp. 6228-6244, Nov. 2017.

[6]   A. Bacci, D. Staglian, E. Giusti, S. Tomei, F. Berizzi, and M. Martorella, "Compressive sensing for interferometric inverse synthetic aperture radar applications," IET Radar, Sonar Navigation, vol. 10, no. 8, pp. 1446–1457, 2016.

[7]   S. Tomei, A. Bacci, E. Giusti, M. Martorella, and F. Berizzi, "Compressive sensing-based inverse synthetic radar imaging imaging from incomplete data," IET Radar, Sonar Navigation, vol. 10, no. 2, pp. 386–397, 2016.

[8]   M. Amin, Ed., Compressive Sensing for Urban Radar. Boca Raton, FL: CRC Press, 2015.

[9]   J. A. Jackson and F. Lee-Elkin, "Exploiting Channel Crosstalk for Polarimetric SAR Compressive Sensing," submitted to IEEE Trans. on Aerospace and Electronic Systems, June 2018, revised Dec 2018.

[10] J. A. Jackson and F. Lee-Elkin, "Channel crosstalk model for fully-polarimetric SAR compressive sensing," in IEEE Radar Conf., Seattle, WA, USA, May 2017, pp. 5445: 1–6.

[11] J. A. Jackson and F. Lee-Elkin, "Polarimetric SAR compressive sensing examples," in IEEE Radar Conf., Oklahoma City, OK, USA, Apr 2018.

[12] J. Becker and J. A. Jackson, "Expansion of dropped-channel PolSAR CS to include a spatial dictionary," in 5th International Workshop on Compressed Sensing applied to Radar, Multimodal Sensing, and Imaging (CoSeRa), Sep 2018.

[13] J. Becker and J. A. Jackson, "Super-Resolution Using Dropped-Channel PolSAR Compressive Sensing," IEEE Radar Conference, Boston, MA, USA, April 22-25, 2019, pp. 5195: 1-6.

[14] C. Casteel and L. Gorham et al., "GOTCHA challenge problem," in Algorithms for Synthetic Aperture Radar Imagery XIV, Proceedings of SPIE, E. G. Zelnio and F. D. Garber, Eds., vol. 6568, 2007.

[15] E. van den Berg and M. P. Friedlander, "Probing the Pareto frontier for basis pursuit solutions," SIAM Journal on Scientific Computing, vol. 31, no. 2, pp. 890–912, 2008.

[16] E. van den Berg and M. P. Friedlander, "SPGL1: A solver for large-scale sparse reconstruction," June 2007, http://www.cs.ubc.ca/labs/scl/spgl1, accessed Jan 2018.

[17] S. R. Cloude, Polarisation: applications in remote sensing. Oxford University Press, 2010.